UDC 541.145. doi: 10.33609/2708-129X.86.10.2020.95-119

INFLUENCE OF CALCINATION TEMPERATURE ON STRUCTURAL-DIMENSIONAL CHARACTERISTICS OF C,S-DOPED TiO_2 NANOSTRUCTURES AND THEIR PHOTOCATALYTIC ACTIVITY IN THE CEFTAZIDIME AND DOXYCYCLINE PHOTODEGRADATION PROCESSES

N. I. Romanovska[1]*, P. A. Manoryk[1], O. V. Selyshchev[2], P. S. Yaremov[1], O. V. Shylzshenko[1], A.V. Terebilenko[3], S. M. Shcherbakov[3], D. R. T. Zahn[2]

[1] L.V. Pisarzevsky Institute of Physical Chemistry, NAS of Ukraine Nauky av. 31, Kyiv 03028, Ukraine
[2] Semiconductor Physics, Chemnitz University of Technology, D-09127 Chemnitz, Germany
[3] M. G. Kholodnyy Institute of Botany, NAS of Ukraine, Tereshchenkivska str. 2, Kyiv 01601, Ukraine
**e-mail: nat.romanovska@gmail.com*

Mesoporous C, S-doped TiO_2 nanostructures were obtained by solvothermal sol-gel method followed by calcination at different temperatures. It was found that with increasing calcination temperature, the crystallite size remains in the same range of 9–10 nm, while the morphology of TiO_2 nanoparticles significantly changes, and the anatase content increases from 42% to 95%. At the same time the nanoparticle size (from 85 to 45 nm), the specific surface area (200–130 m^2/g), the mesoporous area (from 170 to 70 m^2/g), and the carbon (0.80–0.41%) and sulfur (1.39–0.89%) contents decrease. Varying the calcination temperature allows TiO_2 nanostructures to be obtained with a certain balance of these structural-dimensional characteristics that provides high photocatalytic activity in the processes of ceftazidime and doxycycline photodegradation.

Key words: mesoporous C, S- doped TiO_2, thiourea, calcination, photocatalytic activity, antibiotics.

INTRODUCTION. Titanium dioxide (TiO_2) is one of the most promising materials for solving a number of modern technical and technological problems, ensuring the sustainable development of society, including harvesting of solar energy, more efficient mineral fuel consumption, environmental protection, air purification and sterilization [1, 2, 3, 4, 5]**.** This is caused by low cost, high availability, chemical and photocorrosion resistance of the TiO_2 (anatase) semiconductor, the properties of which allow separated charges (electrons and holes, e^-/h^+) to be generated under UV-light irradiation, which are involved in redox processes [1, 2]. Doping and co-doping of TiO_2 by nonmetals (NM=B, C, N, F, S, *etc.*) for obtaining

NM-doped TiO_2 materials is one of the most promising ways to eliminate the inherent TiO_2 shortcomings, such as the wide bandgap (E_g = 3.2 eV for anatase), low efficiency to sunlight (~4%), fast recombination of photogenerated e^-/h^+ pairs, low sorption capacity, *etc.* [1, 2]. In addition, doping also makes it possible to increase the photocatalytic activity (PCA) of TiO_2. According to existing notions, nonmetal (C and/or S) doping can occur in three ways [1, 6]: substitutional doping (when dopant atoms (C [7–9] and/or S [10, 11]) substitute oxygen in the crystal lattice); interstitial doping (when the additive atom (C [7–9] and/or S [10–12]) is in the interplanar space of the crystal lattice and is associated with one or several oxygen atoms in the lattice, which leads to its distortion); and mixed (when both types of doping are realized simultaneously) [8]. At the same time, some dopant atoms may also be included in different functional groups, for example, sulfate [7, 10, 11] or carbonate [8, 9, 13], on the material surface. The implementation of these options depends on the nature of the dopant, the conditions of the doping process, the precursor of the dopant, and the conditions of post-synthetic processing [1, 2, 4, 5]. N>C>S are considered as the strongest dopants, for which all the above types of doping can be realized [1, 4, 5, 6, 12, 14, 15]. Even though the numerous calculations of the energy and electronic states of O 2p, Ti 3d and NM (N 2p, S 3p, *etc.*) of doped anatase (NM-doped TiO_2) using different models and approximations [1, 4, 5, 6, 14–16], as well as the interpretation of experimental results are rather controversial, this makes it possible to assess the state and role of dopant in NM-doped TiO_2 and NM-codoped TiO_2.

In particular, it was shown that the replacement of titanium by sulfur in the crystal lattice of anatase for S-doped and N, S-codoped TiO_2 is more energetically favorable [15] and leads to bandgap narrowing [16]. At the same time, from the thermodynamic stability point of view, S atoms can be localized in both O and Ti sites in S-doped anatase [17]. As a result of the mixing of O 2p, N 2p, S 3p, and Ti 3d states, the bandgap (E_g) decreases and the absorption band edge shifts to higher wavelength (>400 nm). In turn, the PCA (VIS) is higher for N, S-coped TiO_2 than for S-doped TiO_2 or N-doped TiO_2 [15]. Among C-, N-, S - doped TiO_2 [5], C-doped TiO_2 in which carbon enters the crystal lattice in the form of an anion or cation [5] is the most promising photocatalyst due to the overlap of the O 2p and C 1s states near the valence band edge and its redshift in C-doped TiO_2. Other authors [5] disagreed with a decrease in E_g and believe that such a decrease may be very modest. At the same time, an increase for visible light response and PCA (VIS) is associated with the appearance of isolated localized states in the gap, rather than with narrowing it [1, 5, 6]. Carbon states can also overlap with the TiO_2 conduction band due to the rather deep location in the bandgap [15]. For N-doped TiO_2, both substitutional and interstitial localized occupied states are generated in the bandgap, which provides a visible light sensitivity and PCA (VIS) [6].

Simultaneous co-doping often gives more positive results compared to mono-doping due to the manifestation of synergistic effects [1, 4, 5]. From this point of view, thiourea (TU) is of particular interest as a precursor that contains simultaneously C, N, and S. TU and various titanium (IV) compounds can be used as precursors for the synthesis of (NM)-doped TiO_2 materials by "dry" (calcination of mechanical or mechano-chemically treated mixtures)

or "wet" (sol-gel synthesis followed by calcination) methods. It was shown that TiO_2 obtained by NM doping, where NM = (C, N, S) [7], (N, S), [7, 11, 18, 19], (N) [19], (S) [12, 20–22], (C) [8, 9], demonstrate increased PCA (VIS) in various redox processes. However, according to the calculation results and experimental data, the positive doping effect on the visible light sensitivity and PCA does not always lead to a change in the bandgap and the shift of the band edge [1, 5]. So far, intensive discussions are underway on the mechanism of doped TiO_2 photocatalytic response to visible light, and theoretical studies and experimental results are often contradictory. This can be attributed to the variety of synthesis methods for these materials and different calculation methods [5]. Because each factor affecting PCA is difficult to investigate individually, and because photocatalysis is a complex process influenced by many factors, attempts to determine a universal law of the doping effect on PCA have so far been unsuccessful [5].

Besides, doping can take place both inside the TiO_2 lattice and at the photocatalyst surface [5], which is in direct contact with the organic substrate. Therefore, the amount and nature of dopant in the surface layer may significantly affect PCA (VIS). However, the questions of the effect of the precursor concentration (in particular TU) in the sol-gel system on the number and nature of dopant atoms in (NM)-doped TiO_2, their distribution in volume and on the surface, structural and dimensional characteristics and morphology of the obtained material have hardly been addressed. With respect to available experimental results (relative to S^{2-} [10, 11, 19], S^{4+} [12, 19, 20], S^{6+} [21, 23]) the interpretation is not unambiguous.

It is known [25] that the hydrothermal method allows different classes of inorganic materials in the nanocrystalline state to be obtained. The calcination temperature significantly affects the phase composition, morphology, crystallite and particle size, texture, dopant content, and their chemical state under doping of the TiO_2 nanostructures by carbon, nitrogen, and sulfur (NM) [12]. The phase content ratio in (S)-doped TiO_2 critically depends on the calcination temperature [12, 23], the sulfur precursor nature, the amount used in the reaction mixture [12, 21], and the calcination time [23].

In some cases, doped mixed phases show higher photocatalytic activity compared to the corresponding single-phase materials. The optimal anatase/rutile phase ratio for the mixed phases is 75%:25% - 85%:15% [12, 26]. Despite the fact that anatase has a higher photocatalytic activity than rutile, in some cases, doped rutile [27] is more active. Incorporation of dopants, such as sulfate, in TiO_2 stabilizes anatase before transformation into rutile [21] that begins at higher temperatures - 800°C [12, 28], 950 °C [12], and does not end even at 1100°C (48% A + 52 % R) [12].

High calcination temperature in air leads to the formation of sulfuric acid in the structure of TiO_2, in which S atoms are embedded interstitially [12]. There is a certain optimum sulfur content in (S)-doped TiO_2 (0.1-0.3 wt. % S), which provides a reduction of the bandgap (3.15-2.75 eV) and provides a sufficient lifetime of photogenerated charge carriers [24]. The decrease of dopant content with increasing calcination temperature leads to an increase of crystallite and particle sizes (for example, the temperature increase from 200 to 600 °C induces a crystallite size growth from 9 nm to

24.9 nm [21]), resulting in deteriorating the texture characteristics, first of all, a decrease in the surface area [12, 29]. Since a larger particle size and a smaller surface area are known to reduce the number of photogenerated electrons [30, 31], such changes lead to a decrease in photocatalytic activity [1, 2, 30, 31]. Therefore, in order to obtain effective photocatalysts, it is important to choose such a composition of the reaction mixture and a calcination temperature that would provide non-metal-doped fine-crystalline (9-10 nm) anatase, characterized by an optimal balance of nanoparticles of a certain morphology, and a mesoporous structure with a developed surface, which improves the photocatalytic activity of such materials.

The rapid increase in antibiotic consumption in the last decade has led to intensive pollution of natural waters, which contributes to the development of resistance in microorganisms and, consequently, possess a threat to human health and requires high costs for the development of new antibiotics as well as materials and technologies for water purification [31, 32]. Photocatalytic processes that use the energy of sunlight [31, 32] and NM- doped TiO_2 materials as catalysts [1, 5, 6] are promising in this aspect.

The aim of this study was to elucidate the effect of the calcination temperature on the chemical and phase composition, texture, and morphology of TiO_2 nanostructures, obtained from thiourea containing sol-gel systems, and their photocatalytic activity in the doxycycline and ceftazidime antibiotics photooxidation reactions.

EXPERIMENT AND DISCUSSION OF THE RESULTS

Titanium tetrabutoxide (Sigma Aldrich), thiourea (ch.p) (Reachim), acetic acid (ch.p), ethanol (96%), (UKRORGSYNTEZ Ltd.), doxycycline, and ceftazidime (BCPP) were used.

Sulfur and carbon-doped TiO_2 nanostructures were obtained by a modified method [33] by mixing titanium tetrabutoxide with ethanol and thiourea solutions, that were prepared by dissolving 3.4 ml titanium tetrabutoxide in 30 ml anhydrous ethanol and 0.253 g of thiourea in 20 ml of absolute ethanol, followed by addition of 1 ml glacial acetic acid and 1 ml distilled water and stirring vigorously on a magnetic stirrer during 30 minutes. The resulting sol was transferred into a Teflon beaker and subjected to solvothermal treatment (STT) at 120 °C for 24 hours. The resulting precipitate was separated from the mother liquor by centrifugation and washed twice by distilled water and then dried at 100 °C for 12 hours. The obtained powder was calcined at 200, 300, 400, and 450 °C for 3 hours. The samples were labeled as (X) TiO_2 (T_1/T_2), where X is the molar ratio TU/Ti$(OBu)_4$, T_1 is the STT temperature, T_2 is the calcination temperature. The nitrogen and carbon content in the samples was determined using a C, H, N-analyzer "Carlo Erba 1106". The sulfur content was determined using an X-ray fluorescence spectrometer ElvaX.

Diffractograms of the samples were recorded on a Bruker D8 Advance diffractometer using CuK_α radiation. Transmission (TEM) and scanning (SEM) electron micrographs were obtained on microscopes JEM 1230 and JSM-6060 LA (JEOL) at accelerating voltages of 200 kV and 30 kV, respectively. Diffuse reflection spectra were recorded on an Evolution 600 spectrophotometer (Thermo Scientific). FTIR spectra were recorded on a spectrometer Perkin Elmer Spectrum One in KBr pellets with a sample/KBr ratio of 1/100. Nitrogen adsorption/desorption isotherms were measured

by the volumetric method at 77 K on a Sorptomatic 1990 instrument. Before measurements, the samples were degassed for 5 hours at 330 °C. The external specific surface area (S_{ext}) was calculated according to the method described in [34]. Thermoprogrammed desorption with mass spectrometric control (TPD-MS) was performed in a quartz tube connected to a quadrupole mass spectrometer MX7304A (Selmi) with ionization by electrons of 70 eV. The sample in the tube was heated linearly at a rate of 14 °C/min from room temperature to 800 °C. Mass spectra of the gas phase were recorded continuously during heating. X-ray photoelectron spectroscopy (XPS) spectra were recorded using an ESCALAB 250Xi spectrometer (Thermo Scientific) equipped with a monochromatic Al K_α X-ray source ($h\nu$ = 1486.68 eV). The samples were pumped out in a vacuum for at least 24 hours until the base pressure in the chamber reaches $5\text{-}8\times10^{-10}$ mbar. High-resolution spectra were recorded at an analyzer pass energy of 20 eV, providing a spectral resolution of 0.5 eV.

The photocatalytic activity (PCA) of samples calcined at different temperature were investigated under UV and visible light irradiation (respectively PCA (UV) and PCA (VIS)) for the colorless cephalosporin (ceftazidime) and doxycycline antibiotics photodegradation processes. In the absence of a photocatalyst, solutions of ceftazidime and doxycycline remain stable for a long time. PCA (UV) and PCA (VIS) were determined by the conversion degree (R_{60}) for 60 minutes. A portion of the sample was suspended in aqueous solutions of doxycycline (or ceftazidime) with a concentration of 6.5×10^{-5} M at a sample/solution ratio of 1 g/L and left overnight to establish sorption equilibrium. The suspension was irradiated with ultraviolet (λ=365 nm, UV lamp Delux 26W) and visible light (Maxus 8 W lamp, equipped with a light filter that transmits light with $\lambda > 400$ nm), with a radiation intensity near the surface of the suspension of 0.05 mW/cm^2 and 2.0 mW/cm^2, respectively. The light intensity was measured with a 91150V Reference Cell and Meter (Newport) at the distance of 40 cm that corresponds to the distance from the lamp to the surface of the suspension. An aliquot of the suspension was taken at regular intervals, centrifuged for 15 minutes, and absorption spectra were recorded on a spectrophotometer Specord 210 (Analytic Jena). The absence of doxycycline and ceftazidime in the photocatalyst after the photocatalytic experiment was controlled by UV-vis spectra (Evolution 600 (Thermo Scientific)). The content of doxycycline, ceftazidime, and its photodegradation products in the solutions after photocatalysis was monitored by HPLC (liquid chromatograph Waters Alliance E 2695 with UV detector), according to the European Pharmacopoeia (EUROPEAN PHARMACOPOEIA 10.0) and ^{1}H-NMR.

The sol obtained from the reaction mixture containing thiourea after solvothermal treatment contains about 43% (table 1) of the anatase crystalline phase (sample (0.33) TiO_2 (120/0)). Thus, in the diffraction pattern of the obtained samples (fig. 1, curve 1), a set of reflexes at 2θ = 25.2, 37.8, 48.1, 54.0, 54.9, 62.6, 68.9, 70.4, 75.2° can be attributed to the characteristic reflexes of the anatase crystalline phase (JCPDS № 21-1272). As the calcination temperature increased (fig. 1, table 1), the anatase content calculated from the diffraction data gradually increases from 43% for (0.33) TiO_2 (120/0) to 90% for (0.33) TiO_2 (120/450) (Table 1) with a slight increase in the crystallite

size, calculated by the Scherrer equation from 9 nm (for (0.33) TiO_2 (120/0)) to 10 nm (for (0.33) TiO_2 (120/450)). The small narrowing in the characteristic anatase reflexes with increasing calcination temperature (fig. 1) can be explained by the small increase in the anatase crystallite size.

Changes in the chemical composition and nature of the groups that occur with increasing calcination temperature were determined using elemental and thermogravimetric analysis, FTIR, XPS and UV-vis spectroscopy, and TPD MS. According to elemental analysis (table 1), with calcination temperature increase, the carbon content in the samples studied decreases from 0.80% to 0.41% and the sulfur content decreases from 1.39% to 0.89%. No nitrogen is detected in the samples.

Table 1

Structural and dimensional characteristics of samples and the dopants content

Sample	%A	d, nm			% C	% S	E_g, eV
		XRD	TEM	SEM			
(0,33) TiO_2 (120/0)	43	9	8	85	0.80	1.39	3.05
(0,33) TiO_2 (120/200)	77	9		95	0,62	1.24	3.07
(0,33) TiO_2(120/300)	80	9		64	0,53	1.12	3.07
(0,33) TiO_2 (120/400)	85	9		52	0,47	0.98	3.07
(0,33) TiO_2 (120/450)*	90	10	9	45	0.41	0,89	3.07
(0) TiO_2 (120/450)*	85	9			0.45	-	3.09
(0,17) TiO_2 (120/450)*	95	10			0.51	0,48	3.07

*data from [36]

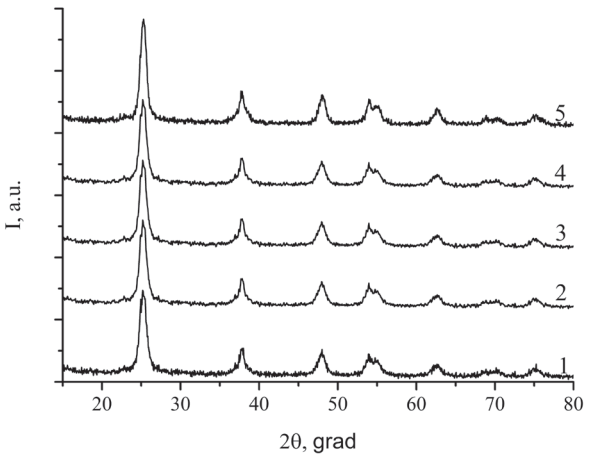

Fig.1 Diffraction patterns of synthesized samples: 1 – (0.33) TiO_2 (120/0); 2 – (0.33) TiO_2 (120/200); 3 - (0.33) TiO_2 (120/300); 4 – (0.33) TiO_2 (120/400); 5 – (0.33) TiO_2 (120/450).

The evolution in the content of anatase in the samples (Table 1) as well as the appearance of carbon and sulfur (Table 1) with calcination temperature increase indicates the presence of an amorphous phase. The amorphous phase can be a modified amorphous titanium inorganic polymer (MATIP), similar to the one described in [35], stabilized with organic (acetate, alcohol, *etc.*) and inorganic (carbonate, sulfate, OH) groups.

The above-mentioned groups, which are present in MATIP, probably, prevent its destruction and anatase crystallization, as well as block the anatase crystallite growth (Table 1) and the anatase to rutile phase transformation.

This trend maintains [36] for the other calcined at 450 °C samples. For example, for (0.17) TiO_2 (120/450) with a crystallite size of 10 nm, the anatase content is 95%. It was previously shown [37] that anatase nanoparticles, which are formed mainly in an acidic medium, are stabilized by the surface adsorbates containing a lot of hydrogen (hydrogenated, hydrogen-rich and hydrated surfaces), which prevent the phase transformation to rutile, and the size and shape of anatase nanoparticles vary only slightly and depends on the surface chemistry (only minor changes in the particles ratio occur). However, both polymorph (anatase and rutile) nanocrystals become elongated in the case of hydrogen-depleted and oxygenated surfaces [37]. Taking into account the fact that the Ti-O-SO_3H groups on the TiO_2 surface are stable up to 600 °C [38], the results of elemental analysis (table 1), TPD MS (fig.4 a, b), and FTIR spectroscopy (fig. 2), allow to assume that the Ti-O-SO_3H and Ti-OH groups are also responsible for maintaining the anatase crystallites size and shape during calcination (200-450 °C).

In the FTIR spectra of (0) TiO_2 (120/0) (fig. 2, curve 1), the bands 1588 and 1440 cm^{-1} (with $\Delta\nu$ = 144 cm^{-1}) are observed, which can be attributed to the valence ν_s and ν_{as} oscillations of acetate groups bridged by CO bonds [35] (or to ν_1 and ν_5 of bidentate and monodentate carbonate [39]). The band at 1630 cm^{-1} is characteristic for deformation oscillations of OH groups in H_2O [39] and/or Ti-OH [18]. The low-intensity bands at 1115, 1090, 1020 cm^{-1} can be attributed to group oscillations of interstitial Ti-O-C bonds [35, 40] and/or oscillations of Ti-O-C butoxyl groups directly associated with titanium [35]. The broad band between 900 - 400 cm^{-1} can be attributed to Ti-O-Ti vibrations of the frame [35, 40, 41]. The broadening of this band is assigned to the amorphous phase. In the FTIR spectra of (0.33) TiO_2 (120/0), (fig. 2, curve 2), these bands are preserved (with a slight shift in their position), and new low-intensity bands appear, which can be attributed to oscillations of C-O bonds ν_1 (1393 cm^{-1}), ν_5 (1598 cm^{-1}) for monodentate and ν_1 (1463 cm^{-1}), ν_5 (1285 cm^{-1}) for bidentate carbonate. The valence symmetric and asymmetric oscillations of S-O bonds ν_3 (1120,1045 cm^{-1}), ν_1 (985 cm^{-1}),ν_2 (469 cm^{-1}) of bidentate sulfate, caused by a decrease in the symmetry of the sulfate ion with high-symmetric T_d to low-symmetric C_{2v}, indicate the formation of bridge bonds with titanium ions. The band ν_3 (1046 cm^{-1}) of monodentate sulfate [39] is identified in similar samples as Ti-O-SO_3H groups [38]. Since the content of the incorporated nonmetals in the obtained samples is quite low, the corresponding bands are low intense and/or manifested themselves as shoulders to the more intense bands in the FTIR spectrum. Because of this, it is difficult to quantify the changes in their intensity during calcination. Nevertheless, a number of trends in their change should be noted.

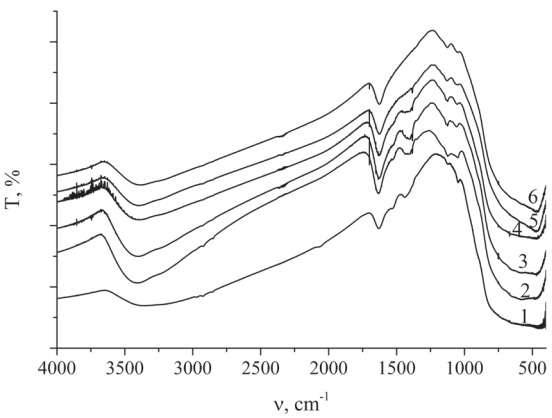

Fig.2 FTIR spectra of the samples: 1 – (0) TiO_2 (120/0); 2 – (0.33) TiO_2 (120/0); 3 - (0.33) TiO_2 (120/200); 4 – (0.33) TiO_2 (120/300); 5 – (0.33) TiO_2 (120/400); 6 – (0.33) TiO_2 (120/450).

As can be seen from fig. 2 (curves 3–6), with calcination temperature increase, there is a tendency to a decrease in the intensity of the valence vibrations band of acetate C-O groups that are associated with a decreasing content of the amorphous phase.

Starting from 300°C, there is also a tendency of a decrease in the intensity of the bands related to monodentate and bidentate carbonate (interstitial carbon).

However, the intensity of the bands, which belong to the bridge (interstitial) sulfate, remains practically unchanged. The intensity of the bands related to the oscillations of OH groups slightly decreases but remains quite high even after calcination at 450°C (fig. 2, curve 6). This may indicate the presence of a large number of OH groups in the sample (0.33) TiO_2 (120/450). The latter fact is important for photocatalysis.

As can be seen in the thermogram (fig. 3a), for (0.33) TiO_2 (120/0) three endoeffects are observed (T_{extr} at 50, 110, 190°C). The two first extrema in the DTG and weight loss in the TG curve can be attributed to the loss of physically and chemically bound water at 50 and 110 °C, respectively. The third effect (190 °C) can be attributed to the loss of residues of organic substances (solvents) that is confirmed by the absence of this effect in the thermogram of the calcined sample (fig. 3 b). An exoeffect with T_{extr} at 370 °C is also observed in the DTA curve that corresponds to the extremum in the DTG and the mass loss in the TG curves. This effect can be associated with the combustion of acetic acid residues and other organic compounds in the modified amorphous titanium oxide inorganic polymer. The course of the DTA curve in the range of 250–650 °C with several extrema that have no correspondence in the DTG curve, may indicate the melting processes. According to the TG this process is accompanied by a slight weight loss in the temperature range 400-650 °C. The extremum in the DTA curve (about 580 °C) can be attributed to the destruction of titanyl sulfate groups on the surface. The similar peak was observed by us previously for samples of doped TiO_2, which were obtained using H_2SO_4 as a sulfur precursor (unpublished results).

In the thermogram of the calcined sample (0.33) TiO_2 (120/450) (fig. 3 b), similarly to (0.33) TiO_2 (120/0) (fig. 3 a), the two endoeffects ($T_{extr.}$ 50, 110 °C) in the DTA curve are observed. They correspond to the extrema on the DTG curve and the weight loss on the TG curve due to desorption of physically and chemically bound water. At higher temperatures, in the thermogram (Fig. 3 b) significant changes in comparison with (0.33) TiO_2 (120/0) (fig. 3 a) are observed. The mass loss in the TG curve in the range of 150–250 °C corresponds to the extremum on the DTG curve (~200 °C), and the exoeffect ($T_{extr.}$ ~215 °C) can be attributed to the combustion of residues of organic compounds that are a part of MATIP. In the temperature range 300–700 °C according to the DTG and TG curves, a barely noticeable monotonic weight loss is observed. In this case, the course of the DTA curve, which has a number of indistinct extrema, indicates the presence of several phase transitions in the temperature range of 300–700 °C. An extremum at $T_{extr.}$ about 730 °C in the DTG and the DTA corresponds to a significant mass loss on the TG curve. Similarly to the peak at 710 °C in the sample (0.33) TiO_2 (120/0) (Fig. 3 a), this effect can be associated with the destruction of the surface Ti-O-SO_3H groups [38] that are formed due to Ti-SH groups oxidation.

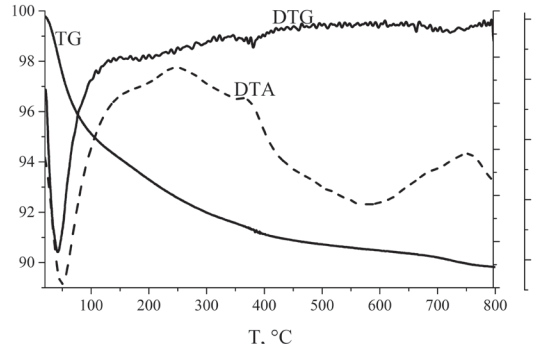

a

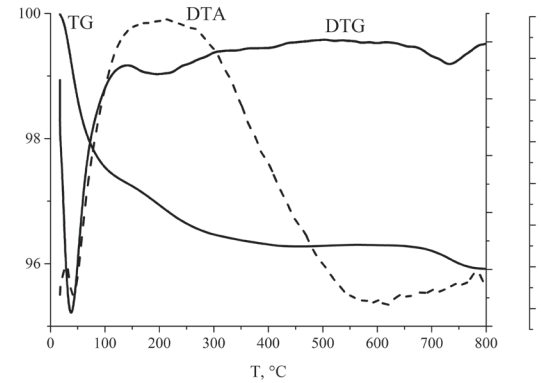

b

Fig. 3 Thermograms of the samples: a – (0.33) TiO_2 (120/0); b – (0.33) TiO_2 (120/450).

In TPD-MS of freshly obtained (0.33) TiO_2 (120/0) (fig. 4 a), maxima of TPD-MS profiles with m/z=28, m/z=34, m/z=44 can be associated with the desorption of CO^+, H_2S^+, and CO_2^+, respectively. As a result of sol-gel synthesis and STT in (0.33) TiO_2 (120/0), the MATIP structure is formed, in which sulfide, carbonate, and, possibly, acetate groups stabilize its structure. The close values of temperatures at which the maxima are observed in the TPD MS profiles m/z=28, m/z=34, m/z=44 in the temperature range 150–500 °C indicate that desorption and destruction processes in MATIP begins with the carbonate bridges destruction (at T_{extr} ~175 °C). The process occurs in two stages. On the first, the CO_2^+, H_2S^+, CO^+, (T_{extr} 203, 216, 230°C, respectively), and at the second, H_2S^+, CO^+, CO_2^+ (T_{extr} 309, 309, 317 °C, respectively) are desorbed. In the temperature range of 500-800°C, extrema in TPD-MS profiles with m/z=44, m/z=34, m/z=28 (at T_{extr} 639, 653, 688 °C) correspond to CO_2^+, H_2S^+, CO^+, respectively. It should be noted that in the TPD MS, the profiles with m/z=18 (H_2O^+) correspond to these three groups of extrema, at T_{extr} 200, 315, and 680°C, indicating the interconnection of desorption processes of CO^+, H_2S^+, CO_2^+, and H_2O^+.

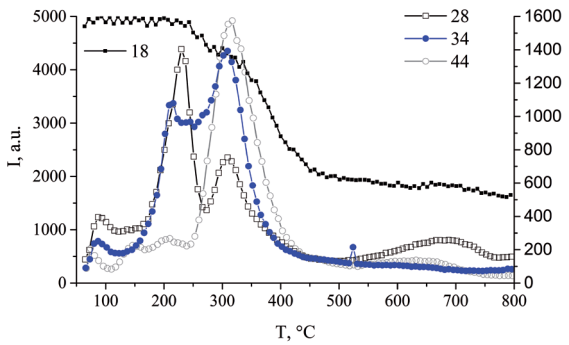

a

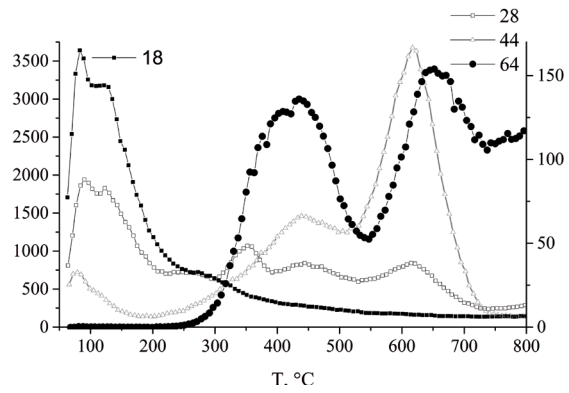

b

Fig.4 TPD-MS spectra of the samples: a – (0.33) TiO_2 (120/0); b – (0.33) TiO_2 (120/450).

Desorption of the lion's share of products in the uncalcined sample (fig. 4 a) occurs in the temperature range of 150-500°C in two stages – at T_{extr} 203, 216, 230 °C (CO_2^+, H_2S^+, CO^+,

respectively) and at T_{extr} ~309, 309, 317 °C (H_2S^+, CO^+, CO_2^+, respectively), probably due to the gradual destruction of monodentate and bridged acetate and sulfide groups.

In TPD-MS of calcined (0.33) TiO_2 (120/450) (Fig. 4 b) in comparison with (0.33) (fig. 4 a), the extrema intensity on TPD MS profiles with m/z=18 (H_2O^+), m/z=28 (CO^+), m/z=44 (CO_2^+) is significantly lower due to the fact that in the process of calcination at 450 °C a significant part of the respective groups is removed from the sample. According to the thermogram of (0.33) TiO_2 (120/0) (fig. 3 a), ~90% of the mass is lost when the sample is heated to 450 °C. Of the five extrema observed on the profile with m/z=28 (CO^+), the first two (at T_{extr} ~110, 254 °C) are probably due to the decomposition of acetate residues. The remaining three (at T_{extr} ~352, 444, 615°C), coinciding with the extrema in the TPD MS profiles with m/z=44 (CO_2^+) at a T_{extr} of about 444, 617 °C, are probably due to the destruction of surface and interstitial carbonate. Next to these three extrema, the peaks in the TPD MS profile with m/z=64 at T_{extr} about 435, 645 °C correspond to the desorption of SO_2^+. Taking into account the fact that the sample (0.33) TiO_2 (120/450) (fig. 3 b) according to X-ray phase analysis contains 95% anatase, the desorption of CO^+, CO_2^+, SO_2^+ at T>300°C can be attributed as to the interstitial also to the surface adhering carbonate and sulfate groups.

Earlier, in the study of TPD of adsorbed H_2S and SO_2 on the surface of TiO_2 [42], it was shown that H_2S and elemental sulfur can be oxidized by titanium dioxide and that the desorption of SO_2 occurs at T_{extr} ~350 °C. According to this, the presence of (0.33) TiO_2 (120/450) in the TPD MS profile (fig. 4 b) with m/z = 64 three extrema (at T_{extr} about ~429, 461, 645 °C) corresponding to the desorption of SO_2^+, may indicate that the main source of SO_2 here are sulfate groups rather than adsorbed SO_2. The sulfate groups are a part of MATIP and stabilize its structure. Because of SO_4^{2-} groups, as well as due to the presence in the TPD MS profiles with m/z=34 (fig. 4 a) for (0.33) TiO_2 (120/0) extrema at T_{extr} ~216°C and 309 °C, we can assume that sulfur, which is the source of H_2S^+, is not physically adsorbed but chemically bound. This fact is consistent with the XPS analysis.

The chemical composition and chemical (oxidation) states of the elements in TiO_2 samples are investigated by means of X-ray photoemission spectroscopy (XPS). The results on the calcined (0.33) TiO_2 (120/450) were reported by us previously [36]. The uncalcined sample (0.33) TiO_2 (120/0) is discussed in detail in this work (fig.5).

As determined from the fragment of the survey XPS spectrum, the surface of the (0.33) TiO_2 (120/0) is composed of titanium and oxygen atoms (30.0 at.% Ti and 52.2 at.% O) and also contains C (17.1 at.%), S (0.36 at.%), and N (0.31 at.%). The atomic Ti/O ratio calculated for the TiO_2 lattice oxygen (the O1s peak at 530.2 eV, fig. 5) is 1:1.74 (± 0.05). Such an oxygen deficiency is mostly caused by the coordination of Ti^{4+} to other functional groups detected in the surface layer, SO_4^{2-}, CO_3^{2-}, OH, *etc.* Fig. 5 shows the high-resolution spectra fitted with Voigt profiles. The peaks at (459.1 ± 0.1) eV and (464.8 ± 0.1) eV correspond to the $Ti2p_{3/2}$ and $Ti2p_{1/2}$ components of the spin-orbit doublet. The separated doublet of lower intensity at (472.3 ± 0.1) and (478.4 ± 0.1) eV stems from plasmon satellites. Thus, the sample contains titanium in a single chemical state, which due to the synthesis conditions, can be unambiguously attributed to Ti^{4+}. It should be noted that the lower oxidation states Ti^{3+}, Ti^{2+}

that usually manifest themselves at lower binding energies to the main Ti^{4+} peak, are not observed in our samples.

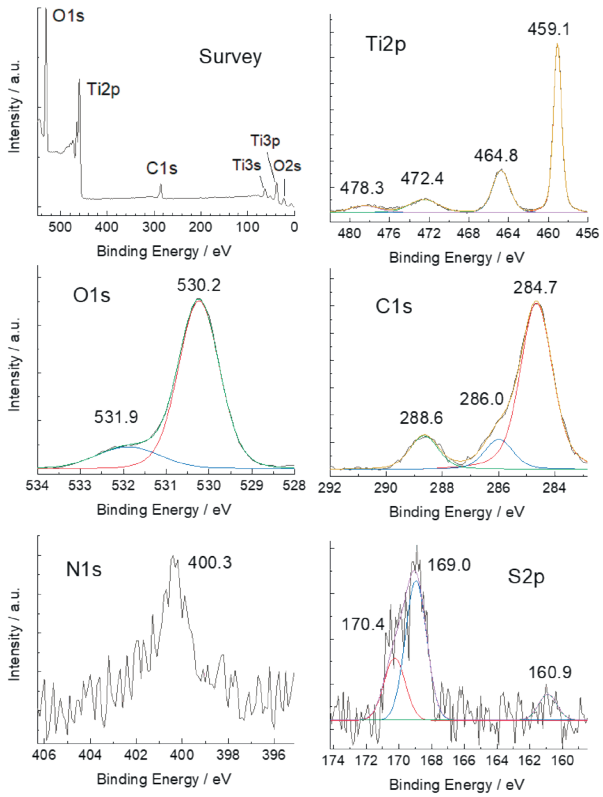

Fig. 5. XPS spectra of the sample (0.33) TiO_2 (120/0).

In the high-resolution O1s XPS spectrum (fig. 5), the intense peak at (530.2 ± 0.1) eV stems from the lattice oxygen of TiO_2 (530.2 eV [9]). The second broader peak at (531.7 ± 0.1) eV can be referred to carbonate (533.0 eV [8]) and sulfate oxygen (531.6 [12]), as well as to oxygen in surface OH (532.0 eV [9], 532.1 eV [21]) and C-O (532.1 eV [8, 21]) groups. Despite the fact that according to the elemental analysis (Table 1), the (0.33) TiO_2 (120/0) does not contain nitrogen (within the sensitivity of the gas chromatography detection), a low intense N1s core-level XPS peak at 400.3 eV is observed. Since XPS is a surface-sensitive method with an information depth less than 10 nm, one can assume that the nitrogen originates from the adsorption of gaseous N_2, NH_3 from the atmosphere by the near-surface layer of the nanostructured sample [7]. Moreover, the surface sensitivity causes the abnormal inflation of the carbon atoms content compared to the CHN analysis data. In the C1s high-resolution XPS spectrum, the most intense peak at (284.8 ± 0.1) eV is mainly formed by the so-called adventitious carbon (typical range 284.5 - 285.0 eV). The latter comes from volatile organic compounds adsorbed on the surface from the atmosphere [8, 9]. Since the total (bulk) carbon content, determined by the elemental CHN analysis for this sample (Table 1), is 0.80%, one can assume that the main share of carbon (fig. 5) is adventitious and does not belong to the volume of the analyzed sample. Two other peaks of approximately the same intensity at (286.3 ± 0.1) eV and (288.8 ± 0.1) eV may correspond to the interstitially incorporated or surface adsorbed carbonate species [8, 9].

It should be noted that the binding energies of Ti2p, O1s, C1s, and N1s peaks detected for (0.33) TiO_2 (120/0) with an accuracy of 0.1 eV coincide with the XPS results on (0.33) TiO_2 (120/450) [36], indicating the proximity of the chemical states of these elements in the samples.

The peaks at (169.0 ± 0.2) eV and (170.4 ± 0.2) eV, revealed in the S2p XPS spectrum (fig. 5), correspond to the $S2p_{3/2}$ and $S2p_{1/2}$ spin-orbit components, respectively. According to the chemical shift, the XPS analysis confirms the S^{6+} oxidation state of sulfur [21].

According to the authors [12], who observed similar results, this indicates the formation of sulfuric acid residues in the structure

of TiO_2 during calcination and the incorporation of S^{6+} sulfur in the structure of TiO_2 (interstitially and on the surface). This is consistent with the FTIR spectroscopy results for the samples (0.33) TiO_2 (120/T_2) (fig. 2), according to which the intensity of the bands attributed to S-O and S=O modes decreases with increasing calcination temperature. This is also confirmed by the results of TPD MS (fig. 4 a, b), where profiles with m/z 64 (SO_2^+) are observed not only for (0.33) TiO_2 (120/450) but also for (0.33) TiO_2 (120/0). In addition, for (0.33) TiO_2 (120/450) (fig. 4 b) in the profile with m/z 64 (SO_2^+), two peaks (T_{extr} ~429 and 652°C) of approximately the same intensity are detected and can be attributed to surface and interstitial sulfate, respectively. The S2p spectrum of the sample after calcination is very close to the uncalcined one. However, the $S2p_{1/2}$ component (170.4 eV) for the (0.33) TiO_2 (120/0) becomes more distinct and exhibits a small shift towards higher binding energies (for comparison, the $S2p_{1/2}$ for the calcined (0.33) TiO_2 (120/450) is at (169.9 ± 0.2) eV [36]). In our opinion, this may be caused by Ti-O-SO_3H groups in the uncalcined sample, revealed by the results of the TGA analysis (fig. 3 a). A low-intense signal about 160.9 eV corresponds to S^{2-} [10, 11, 19] that is consistent with the results of TPD MS (fig. 4a). The intensity of the peak is extremely low, probably, due to the oxidation of the S^{2-} at the surface. Thus, in addition to the CHN analysis, XPS gives reason to believe that the sample (0.33) TiO_2 (120/450) is supplemented with carbon and sulfur.

According to the results of elemental and thermogravimetric analysis, IR, XPS, and TPD MS investigations, the final structure of the calcined samples, in particular (0.33) TiO_2 (120/450), is formed due to the MATIP structure destruction during calcination, which is formed at STT and stabilized by groups (water molecules, carbonate, acetate, sulfate and, possibly, alcohol, which also contains sulfide). According to the XPS and the results of elemental analysis and TPD MS a small number of the permeable nonmetals (C, S), which are part of the interstitial and surface carbonate and sulfate groups, remains in the calcined sample. The MATIP calcination is accompanied by a gradual loss of modifying groups, including sulfate (bridge and surface), which are formed due to sulfide oxidation under calcination that creates the preconditions for the anatase crystallization.

According to the SEM image (fig. 6a) the sample (0.33) TiO_2 (120/0) is in the form of nanoparticles with an average size of 85 nm, consisting of an amorphous phase (58%, table 1) and anatase crystalline sheets (42%, table 1). According to the TEM study (fig. 6 b), the average size of the sheets, is of about 8x7 nm. These sheets also form rectangular units (fig. 6 b, inset) with an average size of 30x8 nm. As the result of calcination at 200 °C, according to the SEM image (fig. 6 c), the average particle size in the sample (0.33) TiO_2 (120/200) increases (up to 95 nm) and their compaction occurs. The size of the anatase crystalline sheets (fig. 6 d) increases from 8x7 nm to 10x8 nm. The anatase sheets aggregate in the rectangular rods with an average size of 200x50 nm (fig. 6 d, inset). After calcination at 300 °C in (0.33) TiO_2 (120/300) the average particle size decreases (up to 64 nm) and their further compaction occur. At the same time, the anatase sheet size decreases from 10x8 nm to 9x8 nm (fig. 6 e), forming aggregates in a shape of rectangular rods (fig. 6 e, inset) with an average size of 20x10 nm. In the SEM image of

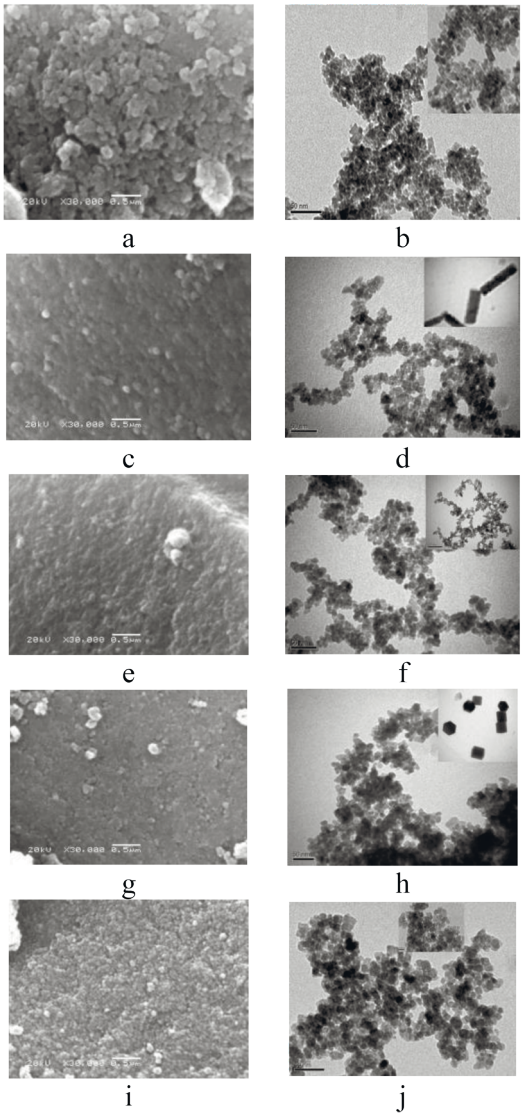

Fig. 6 SEM and TEM images of the samples: a, b – (0.33) TiO_2 (120/0); c, d – (0.33) TiO_2 (120/200); e, f – (0.33) TiO_2 (120/300); g, h – (0.33) TiO_2 (120/400); i, j – (0.33) TiO_2 (120/450).

the sample (0.33) TiO_2 (120/400), calcined at 400°C (fig. 6 g), the particle size decreases to 52 nm, and the particle compactness increases. In the TEM image of this sample (fig. 6 h), the sheets with an average size of 10x9 nm, forming aggregates (fig. 6h, inset) of rectangular (110x170 nm) and hexagonal (65x65 nm) shape, are observed. Calcination at 450 °C ensures a particle size decrease in the SEM image (fig. 6 i) of (0.33) TiO_2 (120/450) to 45 nm and compaction of the material. In the TEM image (fig. 6 j), these anatase crystals are represented by rectangular particles with fused edges of medium size of 10x9 nm, as well as the anatase crystal sheet aggregates in the form of rectangular rods with an average size of 20x14 nm.

The sizes of crystallites (table 1), calculated from diffractograms (fig. 1) and TEM images (fig. 6), are slightly different. According to the calculations from the diffraction patterns (fig. 1), the average particle size in the uncalcined sample (0.33) TiO_2 (120/0) is 8 nm and increases to 9–10 nm in the calcined ones (table 1). According to the TEM images (fig. 6), the size of anatase crystallites of the rectangular sheet shape changes from 8x7nm to 10x8, 9x8, 10x9, and 10x9 nm, depending on the calcination temperature (table 1). The elevating of the crystals results in the formation of the particles of an elliptical shape, probably due to melting of their edges. The differences between the calculation results of X-ray diffraction data and TEM (table 1) may be related to the sheet formation, since the Debye-Scherrer equation is better fitted for the spherical particles. Lamellar morphology is characteristic for facet structures formed in the presence of a dopant such as fluorine [43], which binds to high-energy {001} faces and blocks the anatase crystal growth along the {001} axis. The formation of lamellar anatase crystals in the case of (0.33) TiO_2 (120/T_2) samples can be explained due to the presence of carbonate and sulfate groups on the anatase crystals surface, which, like fluorine, promote the formation of plates

with open faces {001}. Due to the simultaneous presence of the amorphous phase and the anatase crystalline phase in the samples studied (table 1), which according to TEM images is of the sheet shape (fig. 6), we can assume that the nanoparticles, observed in the SEM image (fig. 6) are anatase sheets or sheet agglomerates, covered by amorphous MATIP, *i.e.*, particles of the type "core-shell".

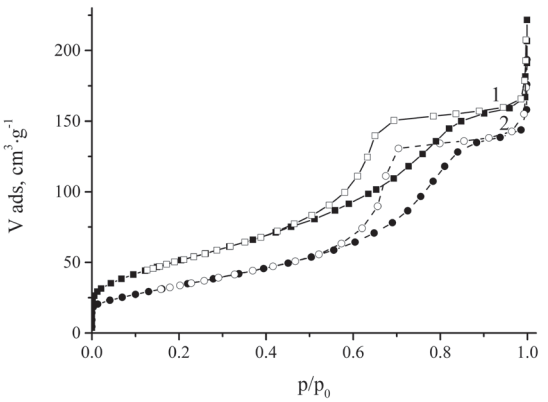

a

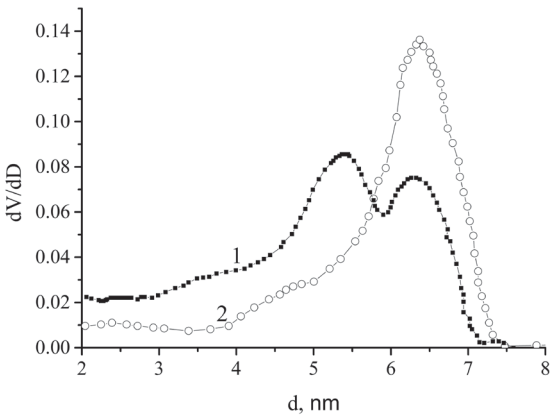

b

Fig. 7 a – Isotherms of samples (0.33) TiO_2 (120/T_2): 1 – (0.33) TiO_2 (120/0); 2 – (0.33) TiO_2 (120/450); b – mesopore size distribution of the sample: 1 – (0.33) TiO_2 (120/0); 2 – (0.33) TiO_2 (120/450).

After the sol-gel synthesis of TiO_2 in the presence of thiourea, followed by solvothermal treatment, mesoporous materials are formed. Isotherms of samples (0.33) TiO_2 (120/0) (fig. 7 a, curve 1) and (0.33) TiO_2 (120/450) (fig. 7 a, curve 2) can be attributed to type IV, which is characteristic for micro-mesoporous materials. The specific surface area (S_{BET}) for the sample (0.33) TiO_2 (120/0) is 190 m^2/g with a mesopore diameter of 5.4 nm, S_{meso} of 170 m^2/g and a total adsorption volume of 0.25 cm^3/g. Nanoparticles form a mesoporous structure, which is formed already at the stage of STT [36]. After calcination at 450°C, the S_{BET} decreases to 130 m^2/g, the total pore volume to 0.22 cm^2/g, the S_{meso} to 70 m^2/g, and the mesopore diameter increases to 6.4 nm. For (0.33) TiO_2 (120/0) on the mesopore distribution curve (fig. 7 b, curve 1) two extrema with maxima at 5.5 and 6.4 nm are observed, and the mesopore average size is 5.4 nm, that indicate the presence of two types of mesopores.

Probably, mesopores of smaller diameter are cavities between spheroidal nanoparticles, which consist of anatase sheets (45%), covered with an amorphous phase, and mesopores of larger diameter are cavities between sheet aggregates (fig. 6 b, inset), in particular, in the form of rods. For the calcined sample (0.33) TiO_2 (120/450), only one extremum (6.4 nm) is observed (fig. 7 b, curve 2) and the average size of mesopores is 6.4 nm. It is possible that the mesopores here are cavities between spheroidal nanoparticles, which consist mainly of anatase crystal sheets (90%) with fused edges (fig. 6, inset), which are tightly adjacent to each other. As a result of calcination, according to TEM images (Fig. 6 d, f, h. j), the 2D anatase crystallite sizes increase, and rectangular (fig. 6 d, f) and hexagonal (fig. 6 h) sheet aggregates, as a result of calcination at 450°C, are compacted and transformed into spheroidal particles. The

specific surface area for (0.33)TiO_2 (120/450) is reduced to 130 m^2/g compared to 190 m^2/g for (0.33)TiO_2 (120/0), which is probably due to a slight increase in the size of the crystallites and the compaction of particles in the volume of the material due to the destruction of the amorphous phase and sintering. A significant increase in the size of the crystallites (table 1) and drastic changes in the texture prevent carbon and sulfur-containing groups. Thus, the calcination temperature is a factor controlling the anatase content, the crystallite and nanoparticle sizes, as well as the textural characteristics of the obtained materials.

For non-calcined sample (0.33) TiO_2 (120/0) (table 1), the bandgap (E_g) value, calculated from the UV-Vis spectra (fig. 8 a, curve 1), is slightly smaller (3.05 eV) compared to E_g (3.2 eV) for bulk anatase. In the UV-vis spectra of samples (0.33) TiO_2 (120/T_2) (fig. 8 b, curves 1-5), the increasing calcination temperature (T_2) induces the bathochromic shift of the absorption band resulting to the slight absorption in the visible region.

In particular, for sample (0.33) TiO_2 (120/450) in the UV-vis spectrum (fig. 8 a, curve 2) the absorption maximum at 320 nm is shifted in comparison with the sample (0.33) TiO_2 (120/0) (fig. 8 a, curve 1). The latter may be due caused by an increase of the amount of titanium ions in an octahedral surrounding, which is characteristic for the anatase crystalline phase [44]. This is consistent with an increase in the anatase content in these samples with calcination temperature increase (table 1).

Besides, for uncalcined sample the absorbance at $\lambda \geq 400$ nm is greater than for the calcined sample (table 1), that is probably due to the presence of more interstitial Ti-O-C groups in (0.33) TiO_2 (120/0), consistent with the elemental analysis results (table 1). According to the latter, the total carbon and sulfur contents decrease with calcination temperature increase.

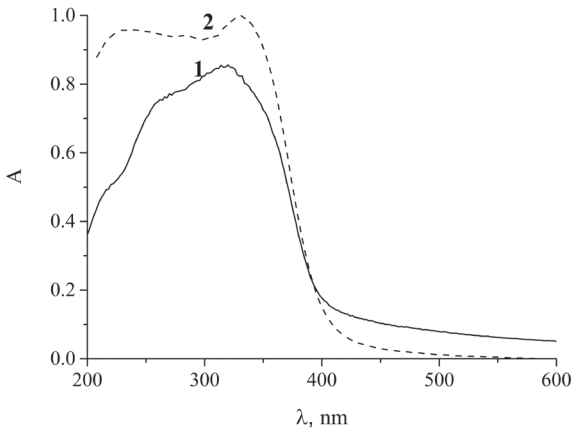

a

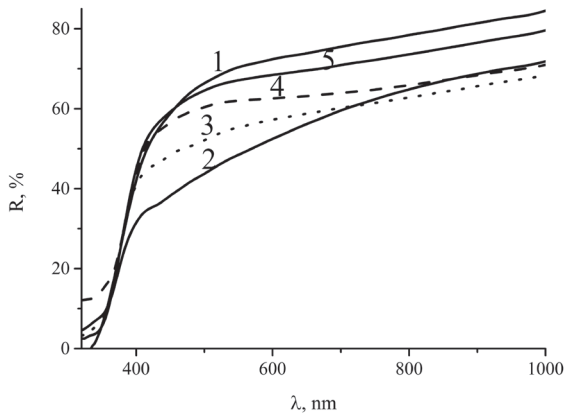

b

Fig. 8. Electronic spectra: a – absorbance spectra of samples: 1 – (0.33) TiO_2 (120/0); 2 – (0.33) TiO_2 (120/450); b - diffusion reflectance spectra of samples (0.33) TiO_2 (120/T_2): 1 – (0.33) TiO_2 (120/0); 2 – (0.33) TiO_2 (120/200); 3 – (0.33) TiO_2 (120/300); 4 – (0.33) TiO_2 (120/400); 5 – (0.33) TiO_2 (120/450);

As can be seen from the evolution of the UV-vis reflectance spectra (fig. 8 b), for the samples (0.33) TiO_2 (120/T_2), an additional absorption in the visible region at $\lambda \geq 400$ nm

is observed after calcination at 200°C (fig. 8 b, curve 2). This may be caused by the interstitial carbonate groups formed in (0.33) TiO_2 (120/200). The intensity of absorption decreases (fig. 8 b, curves 3–5) with calcination temperature increase. At the same time, the nature of the bands changes, which may be associated with the formation of interstitial sulfate groups under these conditions. This is consistent with the results of TPD MS (fig. 4), XPS (fig. 5), FTIR (fig. 2), and TG (fig. 3).

Thus, based on the obtained results (FTIR, XPS, TPD MS, XRD, SEM, TEM, nitrogen adsorption/desorption, elemental analysis), it can be concluded that in the samples (0.33) TiO_2 (120/T_2) the calcination temperature increase (200-450°C) induces an anatase content increase, while amorphous phase content decrease. At that time, the crystallite (of lamellar morphology) size (8–10 nm) slightly increases. The average size of nanoparticles formed by such crystallites together with the amorphous phase decreases (95–45 nm), so as the S_{BET}, S_{meso}, the total adsorption volume, and the interstitial and surface carbonate and sulfate groups content decrease. The bandgap insignificantly narrowed, reaching 3.05–3.07 eV. All these changes lead to a significant effect on the photocatalytic activity of (0.33) TiO_2 (120/T_2) samples.

The effect of calcination temperature on PCA (UV/VIS) of the samples was investigated in the photodegradation reactions of ceftazidime (fig. 9 a) and doxycycline (fig. 9 b). The results are presented in Table 2. As can be seen in fig. 9 a, b, the calcination temperature significantly affects the photocatalytic activity of the obtained samples in the ceftazidime and doxycycline photodegradation processes. The dependence of PCA (VIS) changes on the increasee in calcination temperature, in contrast to the dependence for PCA (UV), shows a dome-shape behaviour (fig. 9 a, b). The conversion of ceftazidime, as well as doxycycline, in the presence of (0.33) TiO_2 (120/T_2) photocatalysts under UV light irradiation increase with calcination temperature increasee and reaches a maximum on the sample (0.33) TiO_2 (120/450) (fig. 9 a, b). The last sample contains the largest amount of anatase (about

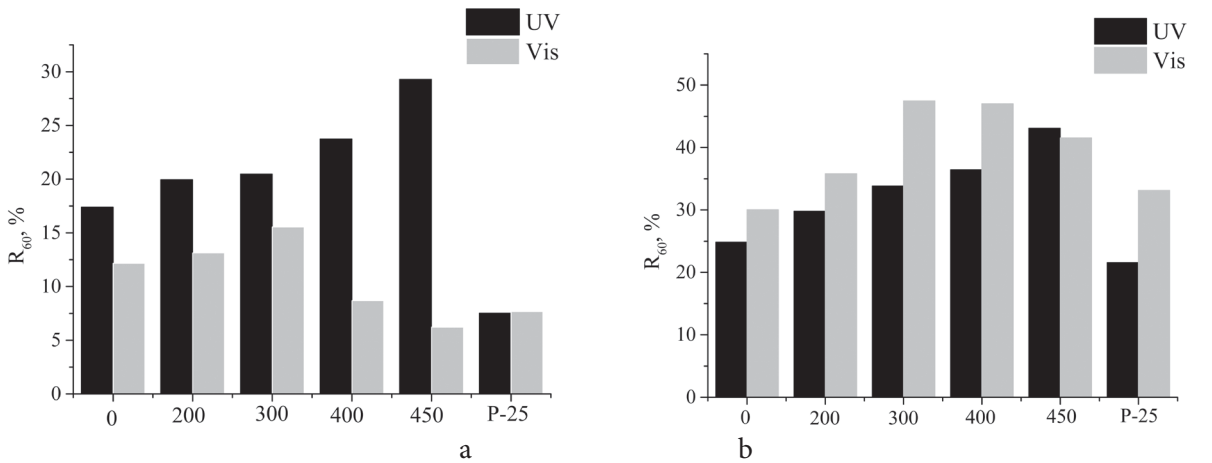

Fig. 9 Conversion degree of: a – ceftazidime; b – doxycycline on the obtained sample under UV (black) and visible (grey) light irradiation

90%) among the studied samples. At the same time, when exposed to visible light, the maximum ceftazidime and doxycycline conversion (fig. 9 a, b) is observed on the sample (0.33) TiO_2 (120/300) with a lower content of anatase (80%) than 90% for (0.33) TiO_2 (120/450). Possibly, the higher photocatalytic activity of the first sample is due to the optimal nanoparticles size (64 nm) and larger number of interstitial Ti-O-C groups, the amount of which increases with an increase in the calcination temperature from 200 to 450°C. It should be noted that a similar trend in PCA (UV/VIS) changes is observed for both stained (doxycycline) and colorless (ceftazidime) antibiotics. Based on this, we can assume that the key positive effect on PCA (UV) is an increasing anatase content in the samples. This effect is also present in the case of PCA (VIS) but taking into account the non-substantial bandgap narrowing (to 3,05–3,07 eV, table 1). This effect is also present in the case of FCA (VIS). However, considering the slight narrowing of the bandgap (table 1) to 3.05–3.07 eV, it is difficult to explain this effect only by the bathochromic shift. Taking into account that the positive doping effect on the visible light sensitivity and PCA does not always lead to a change in the bandgap and shift of the band edge [1, 5] but is a result of interstitial doping and localized states formed in the mid-gap [1, 5, 6], it can be considered that the interstitial carbonate and sulfate groups may play a key role. The ratio between the latter groups changes (increases in favor of the latter) with increasing calcination temperature. Higher PCA (VIS) compared to PCA (UV) of the samples for doxycycline (fig. 9 b) in contrast to ceftazidime (fig. 9 a) photodegradation processes is probably associated with a higher adsorption capacity of these samples relative to doxycycline comparable to ceftazidime (table, 2), as well as the doxycycline photosensitizing effect.

Table 2

Sorption capacity of (0.33) TiO_2 (120/T_2) samples

Sample	Q, 10^{-5} mol/g	
	ceftazidime	doxycycline
(0,33) TiO_2 (120/0)	2.12	4.05
(0,33) TiO_2 (120/200)	1.93	3.64
(0,33) TiO_2(120/300)	2.46	4.57
(0,33) TiO_2 (120/400)	1.95	3.57
(0,33) TiO_2 (120/450)*	1.97	3.78
P-25 Evonik	0.13	0,46

Regardless of the samples calcination temperature, PCA (UV) in the ceftazidime photodegradation process on such samples is more than 3 times higher than the conversion value for Evonik P-25. Probably, this is due to the fact that the content of anatase in these samples is higher than in Evonik P-25 (table 1). In addition, these samples are characterized by a more developed surface and a higher adsorption capacity relative to ceftazidime compared with P-25 (table 2). When irradiated with visible light, the conversion on calcined samples (0.33) TiO_2 (120/T_2) (T_2 = 0, 200, 300°C) is 1.5-2 times higher than the value for Evonik P-25 and is maximum for the sample (0, 33) TiO_2 (120/300). This may be due to the slightly higher adsorption capacity relative to ceftazidime compared to the rest of the samples (Table 2), as well as with the optimal size (~50 nm) of nanoparticles. In addition, the interstitial carbon content in this sample is also higher, which may provide its increased PCA (VIS).

However, it is noteworthy that the PCA (UV/VIS) of (0.33) TiO_2 (120/T_2) samples in the doxycycline photodegradation processes is generally higher (1.5-1.7 times) compared with ceftazidime, which is probably due to the approximately 2 times higher adsorption capacity (Q, mol/g) of the corresponding samples relative to doxycycline compared to ceftazidime (Table 2). For example, PCA (UV) for (0.33) TiO_2 (120/450) is 43.09 and 29.29, respectively, and the average adsorption capacity for doxycycline and ceftazidime is 1.97×10^{-5} mol/g and 4.02×10^{-5} mol/g, respectively. The approximately two times greater adsorption capacity may be the reason for this difference between PCA (UV) relative to doxycycline and ceftazidime.

In contrast to PCA (UV), the PCA (VIS) (conversion, R_{60}) ratio values for the doxycycline and ceftazidime photodegradation processes (R_{60} (dox)/R_{60} (cef)) increases from 2.7 to 6.7 as the calcination temperature of the samples (0.33) TiO_2 (120/T_2). This may be associated not only with the greater adsorption capacity of these samples relative to doxycycline (table 2) but also with changes in the interstitial carbonate and sulfate groups amount and their ratios in (0.33) TiO_2 (120/T_2) and the photosensitization effect of the substrate (doxycycline). These assumptions are confirmed by the results of PCA (UV/VIS) comparison with Evonik P-25 in the doxycycline and ceftazidime photodegradation processes (table 2). In particular, the adsorption capacity for Evonik P-25 to doxycycline (Q=0.49 10^{-5} mol/g) is 3 times higher than to ceftazidime (Q=0.13 10^{-5} mol/g). Noteworthy that PCA (UV) for Evonik P-25 in the doxycycline (R_{60}=21.56%) photodegradation process is approximately also about 3 times higher than in the ceftazidime (R_{60}=7.53%) photodegradation process (table 2). At the same time, the PCA (VIS) is approximately 4.3 times higher. For doxycycline and ceftazidime, R_{60} are 33.12 and 7.66%, respectively. Based on these comparisons, it can be assumed that the PCA (VIS) is affected by another additional factor, namely, the photosensitization effect of the substrate (antibiotic). Therefore, it can be expected that for photodegradation processes of stained antibiotics, like doxycycline, in which the absorption band edge in the UV region enters the visible region, the studied (0.33) TiO_2 (120/T_2) nanostructures will be even better photocatalysts.

From the comparison of the PCA (UV/Vis) values for the samples (0.33) TiO_2 (120/T_2) (table 2), it is seen that PCA (UV) and, especially PCA (VIS), of these photocatalysts are significantly higher in the doxycycline photodegradation processes compared to ceftazidime. The reason for that can be the lower adsorption capacity of these materials and Evonik P-25 to ceftazidime (table 2). This may be due to the ceftazidime's greater hydrophobicity and its molecule larger size, compared to doxycycline, as a result, this substrate is less efficiently adsorbed on the photocatalyst surface. The possible influence of different donor atoms in these antibiotic molecules on the efficiency of their interaction with the surface of the photocatalyst is also not excluded.

An additional factor for the superior photocatalytic activity can be the photosensitization effect of the surface-adsorbed doxycycline, which absorbs in the UV region and contains two intense bands with maxima λ_{max} = 270 nm and λ_{max} = 347 nm, the edge of which enters the visible region. Ceftazidime, in contrast to doxycycline, absorbs light mainly in the UV region of < 300 nm.

It was previously shown [22], that the main reason for the three times higher photocatalytic activity in the methylene blue and phenol photodegradation reactions of N, S-doped TiO_2 samples obtained from titanyl sulfate and thiourea, compared to Degussa P25, is the small anatase crystallite size (5–6 nm). According to the authors [22], this may be due to the synergism of the interaction of sulfate and nitrogen with the TiO_2 lattice. In N, S-doped TiO_2, N-Ti-O and O-Ti-N-O are responsible for the redshift, and the sulfate group acts as a cocatalyst to increase surface acidity and to maintain a high stability of the redox cycles [22]. In the case of TiO_2 samples doped with C, S, obtained by us, the average crystallite size is small (9–10 nm) and both interstitial and surface sulfate groups are present. Therefore, the surface sulfate probably also acts as a cocatalyst and the photocatalysis process. According to the mechanism proposed by the authors [22], it provides for the participation of surface sulfate in the redox transformations ($S^{6+} \leftrightarrow S^{4+}$). The visible light absorption by (0.33) TiO_2 (120/T_2) nanostructures with a small decrease (~0.15 eV) in the bandgap width (table 1) in comparison with pure anatase is provided, mainly, by the interstitial C-O-Ti and S-O-Ti. According to [1, 5, 6], these groups can form localized states between VB and CB, helping to increase the sensitivity to visible light without significantly narrowing the bandgap. The presence of sulfate ions in the (0.33) TiO_2 (120/T_2) sample surface structure that are formed during calcinating may promote the migration of photogenerated electrons, thereby improving the photogenerated charge carriers separation, and inhibition of recombination processes, which improves the photocatalytic activity, as it was observed for N, S-doped [22] and S-doped [21] TiO_2 nanostructures.

As can be seen from the comparison of the PCA (UV/VIS) for (0.33) TiO_2 (120/T_2) samples and (X) TiO_2 (120/450) [36], the optimal calcination temperature is one of the key controlling factors for the structural and dimensional characteristics of doped TiO_2 nanostructures and their photocatalytic activity in the doxycycline and ceftazidime photodegradation processes. Thus, PCA (UV/VIS) for (X) TiO_2 (120/T_2) samples, in which the anatase content increases with increasing calcinating temperature, gradually increases but is smaller compared to samples with a high content of anatase (X) TiO_2 (120/450) (X=0; 0.17; 0.33). At the same time, the PCA (VIS) of the (0.33) TiO_2 (120/300) sample, which is calcined at 300°C, is higher in comparison with all other samples (Table 2), including the best sample (0.17) TiO_2 (120/450), which was obtained at the optimal X=TU/TBT=0.17 ratio in the reaction mixture [36]. Taking into account the above results and assumptions, we can assume that one of the reasons for this is changes in the interstitial dopants content and their ratio, that are achieved at a calcination temperature of 300 °C. This is also consistent with the results of elemental analysis (table 1) and XPS (fig.5).

It should be noted that our (0.33) TiO_2 (120/T_2) samples, containing interstitial and surface carbonate and sulfate groups, show a higher PCA (VIS), compared to those obtained by titanate nanotube with TU calcinating in vacuum at 500 °C encoded by N/S co-doped TiO_2 nanotubes, where N and S replace oxygen in the lattice [11], and which were tested in the methylene blue photodegradation process under close conditions. The PCA (VIS) of the (0.33) TiO_2 (120/T_2) samples is comparable

to the activity in the same process [45] of F,S-doped TiO_2 lamellar nanostructures with a nanoparticle size of 10–15 nm, obtained by solvothermal method (precursors F and S, respectively NH_4F and TU), followed by calcinating at 450 °C and in which F and S are incorporated in the lattice in the oxygen position and show a synergistic effect, that increases the concentration of superoxide and, accordingly, the growth of PCA (VIS) in the methylene blue photodegradation process. Thus, among the (0.33) TiO_2 (120/T_2) samples, the best photocatalytic activity under visible light irradiation in the doxycycline and ceftazidime photodegradation processes is demonstrated by the sample (0.33) TiO_2 (120/300), which is characterized by an anatase content (80%), crystallite size of 9 nm, and spherical nanoparticles (64 nm) and contains interstitial dopants (C, S), and PCA (UV/VIS), that significantly outperforms Evonik P-25.

As can be seen (fig. 9 a, b), the conversion of ceftazidime, as well as doxycycline, under UV light irradiation increases with increasing calcination temperature and reaches a maximum for the sample (0.33) TiO_2 (120/450) (fig. 9 b). Regardless of the calcination temperature of the samples, the PCA (UV) in the photodegradation of ceftazidime is more than 3 times higher than the conversion value for Evonik P-25. At the same time, under visible light irradiation, the maximum doxycycline conversion is observed on the sample (0.33) TiO_2 (120/300) and 1.5-2 times higher than the value for Evonik P-25. It is noteworthy that the PCA (UV/VIS) on the corresponding samples (0.33) C, S doped TiO_2 (120/T_2) in the doxycycline photodegradation is generally higher (1.5 - 1.7 times) in comparison with ceftazidime (Fig. 6 a, b). However, for samples (0.33) TiO_2 (120/T_2) the ratio of PCA (VIS) (conversion after 60 min, R_{60}) for the doxycycline and ceftazidime photodegradation processes (R_{60} (dox)/R_{60} (cef)) increases from 2.7 to 6.7 as the calcination temperature increases (T_2 = 200-450 °C). In contrast, the PCA (UV) for these samples is remained at the same level.

CONCLUSIONS

Interstitially carbon and sulfur-doped TiO_2 nanostructures with high photocatalytic activity in the ceftazidime and doxycycline photodegradation processes were synthesized by sol-gel synthesis followed by solvothermal treatment (120 °C) and calcinating (200–450 °C). With increasing calcination temperature, the anatase content and mesopore diameter (from 5.4 to 6.4 nm) increase, while the amorphous phase content decrease in the obtained samples. The anatase crystallites of lamellar morphology slightly increase in sizes (from 8x7 nm to 10x9 nm). The anatase crystallites, together with the amorphous phase, are arranged in rectangular and hexagonal stacks that form nanoparticles. The average size of the nanoparticles decreases (95-45 nm) along with the decrease in the S_{BET} (190-130 m^2/g), the S_{meso} (170–70 m^2/g), the total adsorption volume (0.25–0.22 cm^3/g), and the carbon and sulfur content, which are a part of the interstitial and surface carbonate and sulfate groups.

Varying the calcination temperature allows TiO_2 nanostructures to be obtained with a certain balance of these characteristics that provides a high photocatalytic activity for these structures not only under ultraviolet irradiation but also under visible light. The key positive effect on the PCA (UV) of the studied samples in doxycycline and ceftazidime photodegradation processes is exerted by the high anatase

content, the large mesopore surface area, and the small crystallite and nanoparticle size. This effect is also present in the case of PCA (VIS), but here the key role is played by the interstitial carbonate and sulfate groups. The content and ratio of these groups decrease with increasing calcination temperature. The higher PCA (VIS) compared to the PCA (UV) of the (0.33) TiO_2 ($120/T_2$) samples to doxycycline, in contrast to the ceftazidime photodegradation process, is associated with the higher adsorption capacity of these samples, and probably with the photosensitizing effect of doxycycline.

The visible light absorption by (0.33) TiO_2 ($120/T_2$) samples is ensured, mainly, by the presence of interstitial C-O-Ti and S-O-Ti with a small decrease (~0.15 eV) in the width of the bandgap compared to pure anatase. The sulfate ions formed during calcination, which are present in the surface structure of C, S-doped TiO_2, promote the photogenerated electron migration, thereby improving the separation of photogenerated charge carriers and inhibition of recombination processes that improves photocatalytic activity.

Thus, the calcination temperature is a factor of controlling the anatase content, crystallite and nanoparticle size, morphology, textural characteristics, and the content of interstitial and surface sulfate and carbonate groups. The balance of these factors ensures their PCA (UV/VIS) in the ceftazidime and doxycycline photodegradation processes. The photocatalytic activity (PCA UV/VIS) of the samples containing carbon and sulfur only in the interstitial and surface groups and not containing (C, S) dopants incorporated directly into the lattice significantly outperform Evonik P-25 and can be used for the antibiotic photodegradation processes under sunlight irradiation.

Acknowledgment

This work was supported by National Academy of Science of Ukraine.

ВПЛИВ ТЕМПЕРАТУРИ КАЛЬЦИНУВАННЯ НА СТРУКТУРНО-РОЗМІРНІ ХАРАКТЕРИСТИКИ C,S-ДОПОВАНИХ TiO_2 НАНОСТРУКТУР ТА ЇХНЯ ФОТОКАТАЛІТИЧНА АКТИВНІСТЬ У ПРОЦЕСАХ ФОТОДЕГРАДАЦІЇ ЦЕФТАЗИДИМУ ТА ДОКСИЦИКЛІНУ

Н. І. Романовська[1]*, П. А. Манорик[1], О. В. Селищев[2], П. С. Яремов[1], О. В. Шульженко[1], А. В. Теребіленко[3], С. М. Щербаков[3], Д. Р. Т. Цан[2]

[1]Інститут фізичної хімії ім. Л. В. Писаржевського НАН України, просп. Науки, 31, Київ 03028, Україна

[2]Фізика напівпровідників, Технічний університет міста Кемніц, Кемніц, 09127, Німеччина

[3]Інститут ботаніки ім. М. Г. Холодного НАН України, вул. Терещенківська, 2, Київ 01601, Україна

**e-mail: nat.romanovska@gmail.com*

Мезопористі C, S-доповані наноструктури TiO_2 одержано сольвотермальним золь-гель методом з наступним кальцинуванням за різних температур. Встановлено, що зі зростанням температури кальцинування при незначних змінах розмірів кристалітів (9–10 нм) зростає вміст анатазу (з 42% до 95%), зменшується розмір наночастинок (з 85 до 45 нм), питома площа поверхні (200–130 $м^2/г$) та площа мезопор (з 170 до 70 $м^2/г$), зменшується вміст вуглецю (0,80–0,41%) та сірки (1,39–0,89%), відбуваються

кардинальні зміни морфології наноструктур TiO_2. Показано, що варіювання температури кальцинування дозволяє одержати наноструктури TiO_2 з певним балансом цих характеристик, який забезпечує їхню високу фотокаталітичну активність у процесах фотодеградації цефтазидиму та доксицикліну при опроміненні не лише ультрафіолетовим, а й видимим світлом.

Ключові слова: мезопористий C, S-допований TiO_2, тіосечовина, кальцинування, фото каталітична активність, антибіотики.

ВЛИЯНИЕ ТЕМПЕРАТУРЫ КАЛЬЦИНИРОВАНИЯ НА СТРУКТУРНО-РАЗМЕРНЫЕ ХАРАКТЕРИСТИКИ C,S-ДОПИРОВАННЫХ TiO_2 НАНОСТРУКТУР И ИХ ФОТОКАТАЛИТИЧЕСКУЮ АКТИВНОСТЬ В ПРОЦЕССАХ ФОТОДЕГРАДАЦИИ ЦЕФТАЗИДИМА И ДОКСИЦИКЛИНА

Н. И. Романовская[1]*, П. А. Манорик[1], А. В. Селищев[2], П. С. Яремов[1], А. В. Шульженко[1], А. В. Теребиленко[3], С. Н. Щербаков[3], Д. Р. Т. Цан[2]

[1]Институт физической химии им. Л. В. Писаржевского НАН Украины, просп. Науки, 31, Киев 03028, Украина

[2]Физика полупроводников, Технический университет города Кемница, Кемниц 09127, Германия

[3]Институт ботаники им. М. Г. Холодного НАН Украины, ул. Терещенковская, 2, Киев 01601, Украина

**e-mail: nat.romanovska@gmail.com*

Мезопористые C, S-допированные наноструктуры TiO_2 получены сольвотермальным золь-гель методом с последующим прокаливанием при различных температурах. Установлено, что с ростом температуры кальцинирования при незначительных изменениях размеров кристаллитов (9–10 нм) увеличивается содержание анатаза (с 42% до 95%), уменьшается размер наночастиц (с 85 до 45 нм), удельная площадь поверхности (200–130 $м^2/г$) и площадь мезопор (с 170 до 70 $м^2/г$), уменьшается содержание углерода (0,80–0,41%) и серы (1,39–0,89%), происходят кардинальные изменения морфологии наноструктур TiO_2. Показано, что варьирование температуры кальцинирования позволяет получить наноструктуры TiO_2 с определенным балансом этих характеристик, обеспечивающих их высокую фотокаталитическую активность в процессах фотодеградации цефтазидима и доксициклина при облучении не только ультрафиолетовым, но и видимым светом.

Ключевые слова: мезопористый C, S-допированный TiO_2, тиомочевина, кальцинирование, фотокаталитическая активность, антибиотики.

REFERENCES

1. Etacheri V., Di Valentin C., Schneider J., Bahnemann D., Pillai S.C. Visible-light activation of TiO_2 photocatalysts: Advances in theory and experiments. *Journal of Photochemistry and Photobiology C: Photochemistry Reviews*. 2015. **25**: 1.
2. Pelaez M., Nolan N.T., Pillai S.C., Seery M.K., Falaras P., Kontos A.G., Dunlop P.S.M., Hamilton J.W.J., Byrne J.A., O'Shea K., Entezari M.H., Dionysiou D. D. A review on the visible light active titanium dioxide photocatalysts for environmental applications. *Applied Catalysis B: Environmental.* 2012. **125**: 331.
3. Nam Y., Lim J.H., Ko K.C., Lee J.Y. Photocatalytic activity of TiO_2 nanoparticles: a theoretical aspect. *Journal of Material Chemistry. A*. 2019. **7**: 13833.
4. Li W. Influence of electronic structures of doped TiO_2 on their photocatalysis. *Physica Status Solidi RRL*. 2014. **1**.: 1.
5. Cui Y., Du H., Wen L. Invited review doped-TiO_2 photocatalysts and synthesis method to prepare TiO_2 films. *Journal of Materials Science and Technology*. 2008. **24**: 675.
6. Di Valentin C., Pacchioni G., Selloni A., Livraghi S., Giamello E. Characterization of paramagnetic species in N-doped TiO_2 powders by EPR spectroscopy and DFT calculations. *The Journal of Physical Chemistry B.* 2005. **109**: 11414.
7. Zhou M., Yu J. Preparation and enhanced daylight-induced photocatalytic activity of C,N,S-tridoped titanium dioxide powders. *Journal of Hazardous Materials*. 2008. 152: 1229.
8. Wu X., Yin S., Dong Q., Guo C., Li H., Kimura T., Sato T. Synthesis of high visible light active carbon doped TiO_2 photocatalyst by a facile calcination assisted solvothermal method. *Applied Catalysis B: Environmental* 2013. **142-143**: 450.
9. Palanivelu K., Im J. S., Lee Y.-S. Carbon doping of TiO_2 for visible light photo catalysis. *Carbon science*. 2007. **8** (3): 214.
10. Lim S.P., Pandikumar A., Lim H.N., Ramaraj R., Huang N.M. Boosting photovoltaic performance of dye-sensitized solar cells using silver nanoparticle-decorated N, S-Co-doped-TiO_2 photoanode. Scientific Reports. 2015. **5**: 11922.
11. Yan G., Zhang M., Hou J., Yang J. Photoelectrochemical and photocatalytic properties of N+S co-doped TiO_2 nanotube array films under visible light irradiation. *Materials Chemistry and Physics*. 2011. **129** (1-2): 553.
12. McManamon C., O'Connell J., Delaney P., Rasappa S., Holmes J.D., Morris M.A. A facile route to synthesis of S-doped TiO_2 nanoparticles for photocatalytic activity. *Journal of Molecular Catalysis A: Chemical*. 2015. **406**: 51.
13. Liu B, Liu L.-M., Lang X.-F., Wang H.-Y., Lou X.W., Aydil E.S. Doping high-surface-area mesoporous TiO_2 microspheres with carbonate for visible light hydrogen production. *Energy Environmental Science*. 2014, **7**: 2592.
14. Matsushima S., Takehara K., Yamane H., Yamada K., Nakamura H., Arai M., Kobayashi K. First-principles energy band calculation for undoped and S-doped TiO_2 with anatase structure. Journal of Physics and Chemistry of Solids. 2007. **68**: 206.
15. Asahi R., Morikawa T., Ohwaki T., Aoki K., Taga Y. Visible-Light Photocatalysis in Nitrogen-Doped Titanium Oxides. Science. 2001. **293**: 269.

16. Hamal D.B., Klabunde K.J. Synthesis, characterization, and visible light activity of new nanoparticle photocatalysts based on silver, carbon, and sulfur-doped TiO_2. *Journal of Colloid and Interface Science*. 2007. **311**: 514.
17. Jia L., Wu C., Li Y., Han S., Li Z., Chi B., Pu J., Li J. Enhanced visible-light photocatalytic activity of anatase TiO_2 through N and S codoping. *Applied Physics Letters*. 2011. **98**: 211903.
18. Naik B., Parida K.M., Gopinath C.S. Facile synthesis of N- and S-incorporated nanocrystalline TiO_2 and direct solar-light-driven photocatalytic activity. *The Journal of physical chemistry C.* 2010. **114**:19473–19482.
19. Pany S., Naik B., Martha S., Parida K. Plasmon induced nano Au particle decorated over S,N-modified TiO_2 for exceptional photocatalytic hydrogen evolution under visible light. *Applied Material and Interfaces*. 2014. **6**: 839.
20. Ohno T., Akiyoshia M., Umebayashi T., Asai K., Mitsui T., Matsumura M. Preparation of S-doped TiO_2 photocatalysts and their photocatalytic activities under visible light. *Applied Catalysis A: General*. 2004. **265**. 115.
21. Szatmáry L., Bakardjieva S., ˇSubrt J., Bezdiˇcka P., Jirkovsk´y J., Bastl Z., Brezová V., Korenko M. Sulphur doped nanoparticles of TiO_2. *Catalysis Today*. 2011. **161**(1): 23.
22. Esquivel-Escalante K., Nava-Mendoza R., Velázquez-Castillo R. Crystal structure determination of the S/TiO_2 system and the correlation with its photocatalytic properties. *Journal of Nanoscience and Nanotechnology*. 2016. **16**: 967.
23. Baeissa E.S. Synthesis and characterization of sulfur-titanium dioxide nanocomposites for photocatalytic oxidation of cyanide using visible light irradiation. *Chinese Journal of Catalysis*. 2015. **36**. 698.
24. Byrappa K., Yoshimura M. Handbook of Hydrothermal Technology. (William Andrew Publishing, 2001).
25. Bickley R.I., Gonza´lez-Carren˜o T., Lees J.S., Palmisano L., Tilley R.J.D. A structural investigation of titanium dioxide photocatalysts. *Journal of Solid State Chemistry*. (1999). **92**. 178.
26. Liu H., Gao I. (Sulfur,Nitrogen)-codoped rutile-titanium dioxide as a visible-light-activated photocatalyst. *Journal of American ceramic society*. (2004). **87**: 1582.
27. Tong T., Zhang J., Tian B., Chen F., He D. Preparation and characterization of anatase TiO_2 microspheres with porous frameworks via controlled hydrolysis of titanium alkoxide followed by hydrothermal treatment. *Materials Letters*. (2008). **62**: 2970.
28. Tian H., Ma J., Li K., Li J. Hydrothermal synthesis of S-doped TiO_2 nanoparticles and their photocatalytic ability for degradation of methyl orange. *Ceramics International.* (2009). **35**. 1289.
29. Fresno F., Coronado J.M., Tudela D., Soria J. Influence of the structural characteristics of $Ti_{1-x}Sn_xO_2$ nanoparticles on their photocatalytic activity for the elimination of methylcyclohexane vapors. *Applied Catalysis. B.* (2005). **55**: 159.
30. Anpo R., Shima T., Kodama S., Kubokawa Y., Photocatalytic hydrogenation of propyne with water on small-particle titania: size quantization effects and reaction intermediates. *The Journal of physical chemistry*. (1987). **91**: 4305.
31. Cao M., Wang P., Ao Y., Wang C., Hou J.,

Qian J. Visible light activated photocatalytic degradation of tetracycline by a magnetically separable composite photocatalyst: Graphene oxide/magnetite/cerium-doped titania. *Journal of Colloid and Interface Science* (2016). **467**: 129.

32. Borghi A.A., Silva M.F., Arni S.Al, Converti A., Palma M. S. A. Doxycycline degradation by the oxidative Fenton process. *Journal of Chemistry*. (2015). 2015. Article ID 492030, 9 pages http://dx.doi.org/10.1155/2015/492030.
33. Yang G., Yan Z., Xiao T. Low-temperature solvothermal synthesis of visible-light-responsive S-doped TiO_2 nanocrystal. *Applied Surface Science*. (2012). **258**: 4016.
34. Chen F, Xu XJ, Shen S, Kawi S, Hidajat K. Microporosity of SBA-3 mesoporous molecular sieves. *Microporous and Mesoporous Material*. (2004). **75**(3): 231.
35. Doeuff S, Henry M., Sanchez C., Livage J. Hydrolysis of titanium alkoxides: Modification of the molecular precursor by acetic acid. *Journal of non-crystalline solids* (1987). **89**: 206.
36. Romanovska N.I., Manoryk P.A., Selyshchev O.V., Ermokhina N.I., Yaremov P.A., Grebennikov V.M., Shcherbakov S.M., Zahn D.R.T. Effect of the Modification of TiO_2 with Thiourea on its Photocatalytic Activity in Doxycycline Degradation. *Theoretical and Experimental Chemistry*. (2020). **56**: 183.
37. Barnard A.S., Curtiss L.A. Prediction of TiO_2 nanoparticle phase and shape transitions controlled by surface chemistry. *Nano Letters*. (2005). **5** (7): 1261.
38. Manoryk P.A., Lampeka Ya.D., Ermokhina N.I., Tsymbal L.V., Telbiz G.M., Gurtovyi R.I. Functional Titanium Dioxide-Derived Materials of Different Morphology and Metal–Organic Framework Compounds. *Theoretical and Experimental Chemistry*. (2017). **53**: 349.
39. Nakamoto K. Infrared spectra of inorganic and coordination compounds. (M. «Мир», 1966) [In Russian].
40. Nishikiori H., Hayashibe M., Fujii T. Visible light-photocatalytic activity of sulfate-doped titanium dioxide prepared by the sol–gel method. *Catalysts*. (2013). **3**: 363.
41. Enríquez J.M.H., Lajas L.A.C., Alamilla R.G., Martín E.Á.S., Alamilla P.G., Handy E.B., Galindo G.C., Serrano L.A.G. Synthesis of solid acid catalysts based on TiO_2 -SO_4^{2-} and Pt/TiO-SO_2-applied in n-hexane isomerization. *Open Journal of Metal.* (2013). **3**: 34.
42. Chen Y., Jiang Y., Li W., Jin R.,Tang S., Hu W. Adsorption and interaction of H_2S/SO_2 on TiO_2. *Catalysis Today*. (1999). **50**: 39.
43. Han X., Kuang Q., Jin M. Synthesis of titania nanosheets with a high percentage of exposed (001) facets and related photocatalytic properties. *Journal of the American Chemical Society*. (2009). **131** (9): 3152.
44. Eimer G.A., Casuscelli S.G., Ghione G.E., Crivello M.E., Herrero E.R. Synthesis, characterization and selective oxidation properties of Ti-containing mesoporous catalysts. *Applied Catalysis A: General. (2006)*. **298:** 232.
45. Yang G., Jiang Z., Shi H., Jones M.O, Xiao T., Edwards P.P, Yan Z. Study on the photocatalysis of F-S co-doped TiO_2 prepared using solvothermal method. *Applied Catalysis B: Environmental.* (2010). **96**: 458.

Стаття надійшла 21.09.2020.